

3D Printing of Hydrogel/BaTiO₃ Composite Scaffolds with Highly Improved Mechanical, Electrical, and Degradable Properties

Yue Zhang^{1,2}, Jinhan He^{1,2}, Jin Su^{1,2,*}, Annan Chen^{3,4}, Yinjin Li^{1,2}, Yifei Li^{1,2}, Chunze Yan^{1,2} and Yusheng Shi^{1,2,*}

¹State Key Laboratory of Materials Processing and Die & Mould Technology, School of Materials Science and Engineering, Huazhong University of Science and Technology, Wuhan 430074, China

²Engineering Research Center of Ceramic Materials for Additive Manufacturing, Ministry of Education, Wuhan 430074, China

³Centre for Advanced Structural Materials, Department of Mechanical Engineering, City University of Hong Kong, Hong Kong 999077, China

⁴Centre for Advanced Structural Materials, City University of Hong Kong Shenzhen Research Institute, Greater Bay Joint Division, Shenyang National Laboratory for Materials Science, Shenzhen 518057, China

Abstract: In clinical practice, the restoration of cartilage injury is a tough task. And manufacturing degradable cartilage scaffolds with strong mechanical properties and electrical activity remains a significant issue. In this study, the hydrogel/BaTiO₃ composite scaffolds with greatly improved mechanical, electrical, and degradable properties were formed by digital light processing 3D printing. We found that the addition of BaTiO₃ powders enabled the significant improvement of the compressive strength (212.8 kPa) and energy absorption (32.0 mJ/m³), which were as three and six times as those of pure hydrogel scaffolds, respectively. Besides, the composite scaffolds showed a voltage output of above 100 mV, which was two orders of magnitude higher than that of pure hydrogel scaffolds. This voltage output allows for the simulation of electrical microenvironment in native tissues that promote cartilage regeneration and remodeling. Finally, the degradation rate of the composite scaffolds reached 7.1% after 14 days of simulated body fluid (SBF) immersion, while that of the pure hydrogel scaffolds was only 2.8%. This study provides insight into the fabrication of high-performance functional scaffolds for treating cartilage defect.

Keywords: 3D printing, Hydrogel/BaTiO₃ scaffold, Mechanical property, Electrical property, Degradability.

1. INTRODUCTION

The repair and regeneration of articular cartilage injury is one of the challenges facing orthopedic clinical treatment [1, 2]. The advent of bone tissue engineering (BTE) presents an ideal therapeutic strategy for the repair of cartilage defects [3]. As one of the key elements of BTE, cartilage scaffold, offering necessary mechanical and biological microenvironment for cell proliferation and differentiation [4], has become one of the forefronts of cartilage repair research at home and abroad [5]. Hydrogels have been widely used in the manufacture of cartilage scaffolds due to their similar properties to cartilage tissue, such as permeability, moisture retention and biodegradability [6-10]. However, the poor shape retention performance of hydrogel materials and the high complexity of natural cartilage structures make it a great challenge for traditional methods to fabricate high-performance biomimetic cartilage scaffolds [11-14].

Additive manufacturing (3D printing) technology uses computer-aided design (CAD) to print the entity layer by layer according to the pre-designed structure,

which is especially suitable for manufacturing complex structures [15-17]. 3D printing techniques include stereo lithography appearance (SLA), direct ink writing (DIW), two-photon polymerization (2PP) and so on [18-20]. Kajsa *et al.* [21] used DIW technology to achieve cell-based printing of human cartilage cells based on nanocellulose. Shi *et al.* [22] successfully created a scaffold that is both physically and functionally optimized through 3D printing to treat cartilage damage. Digital light processing (DLP) is a representative additive manufacturing technology based on ultraviolet lithography, which is characterized by high molding precision and fast molding speed [23, 24]. As long as the bioink has photocuring properties, it can be processed by DLP [25]. Chen *et al.* [26] obtained ECM/GelMA/exosome scaffolds using DLP printing technology which could enhance chondrocyte migration. The biological function of hydrogel scaffolds created using 3D printing technology, however, is single. The vast majority of them concentrate on mechanical microenvironment reconstruction while ignoring the equally essential electrical microenvironment.

Human bone tissue is reported to be a natural piezoelectric body that generates an endogenous electric field (*i.e.*, the physiological electric microenvironment) through force-electric conversion [27], which is essential for regulating metabolic

*Address correspondence to this article at the State Key Laboratory of Materials Processing and Die & Mould Technology, School of Materials Science and Engineering, Huazhong University of Science and Technology, Wuhan 430074, China; E-mail: jinsu@hust.edu.cn; shiyusheng@hust.edu.cn

processes such as bone formation, structural remodeling, and bone repair [28-32]. Nguyen's team [33] designed a piezoelectric polymer sheet scaffold made of poly-L lactic acid (PLLA) nanofibers for the repair of knee cartilage in rabbits. They discovered that a weak but stable electric field at the joint is essential to cartilage growth. As a result, the physiological electric microenvironment plays a significant role in cartilage repair [34, 35]. Barium titanate (BaTiO₃, BTO) is a biocompatible piezoelectric ceramic that has attracted a lot of attention in recent years because of its high piezoelectric coefficient and approved biocompatibility [36]. However, at present, few reports on relevant studies of the additive manufacturing of cartilage scaffolds can reconstruct the physiological electric microenvironment at the moment [37], and the regulatory mechanism of the electric microenvironment of electroactive complex scaffolds remains unclear.

In this study, a method of additive manufacturing of hydrogel/BaTiO₃ composite cartilage scaffolds with high mechanical strength and adjustable electrical activity was proposed. A hydrogel/BaTiO₃ composite bioink with high stability and ultraviolet light (UV) curable properties was developed, and its rheological and photocurable properties were characterized. The composite hydrogel/BaTiO₃ scaffold was formed by a DLP 3D printer, and its mechanical and electrical properties were systematically characterized. Finally, to confirm the composite scaffolds' degradation, *in vitro* degradation tests were carried out. Results revealed that our hydrogel/BaTiO₃ composite scaffolds have much higher mechanical characteristics than pure hydrogel, which resemble human cartilage. Furthermore, the composite scaffolds have good piezoelectric capabilities and can generate a voltage output of 100mV. The composite scaffolds are biodegradable, with a disintegration rate of 7.1% after 14 days of SBF immersion.

2. MATERIAL AND METHODS

2.1. Materials

BaTiO₃ (BTO, purity 99.9%) powders were purchased from Sigma-Aldrich (Shanghai, China). Poly (ethylene glycol) diacrylate (PEGDA, average molecular weight 600) and polyvinyl alcohol (PVA, alcoholysis degree 99%) were purchased from Aladdin (Shanghai, China). Lithium Phenyl (2,4,6-trimethylbenzoyl) phosphinate (LAP, purity 99%) was provided by SinoBioPrint Biotech Ltd (Shanghai, China). Tartrazine (purity 85%) was obtained from Sigma-Aldrich (Shanghai, China). Phosphate buffered saline (PBS, pH=7.4) was obtained from Biosharp Life

Sciences (Anhui, China). Simulated body fluid (SBF, pH=7.4) was purchased from Phygene Life Sciences Company (Fujian, China).

2.2. Preparation of Bioinks

PEGDA (20 vol.%) and PVA (5 vol.%) were dissolved in deionized water supplemented with lithium Phenyl (2,4,6-trimethylbenzoyl) phosphinate (LAP) ((0.5 wt.%) and tartrazine (0.025 wt.%). Then, BTO powders of 0, 1.0, 2.5, and 5.0 wt.% were added into the above solutions and thoroughly mixed to produce the UV-curable bioinks, denoted as PP, PP/1%BTO, PP/2.5%BTO and PP/5%BTO, respectively.

2.3. Fabrication of Scaffolds

The CAD models were designed as gyroid-type TPMS structures which can be modeled by Matlab software according to the following parametric Eq. (2.1) [38]:

$$\sin\left(\frac{2\pi}{a}x\right)\cos\left(\frac{2\pi}{a}y\right) + \sin\left(\frac{2\pi}{a}y\right)\cos\left(\frac{2\pi}{a}z\right) + \sin\left(\frac{2\pi}{a}z\right)\cos\left(\frac{2\pi}{a}x\right) = t \quad (2.1)$$

where a means the cubic cell length, and t represents the physical volume fraction of TPMS. The side length of the cubic gyroid structural model was 10 mm, and the relative density was 40% ($a=2\text{mm}$, $t=0.4$). Then, the model was sliced by the 10 Dim software with slice layer thickness setting as 25 μm and imported into the DLP printer (AUTOCERA-R, Beijing TenDimensions Technology Co., Ltd., China). The Beer-Lambert model mathematically analyzed the dependency between the curing depth and exposure energy, given by Eq. (2.2) [39]:

$$C_d = D_p \ln E_i - D_p \ln E_c \quad (2.2)$$

where C_d is the curing depth, D_p is the penetration depth, E_i is the actual exposure energy, and E_c is the critical energy. A micrometer was used to measure the curing depth of the bioinks. The PP, PP/1%BTO, PP/2.5%BTO and PP/5%BTO groups were printed with the exposure energy of 240, 300, 320, 360 mJ/cm^2 .

2.4. Characterization Measurements

The particle size of the BTO powders was determined by a laser particle size analyzer (LPSA, Mastersizer 3000, Malvern, UK). The morphology of BTO powders and scaffolds was characterized by a thermal scanning electron microscope (SEM, JSM-7600F, Nippon Electronics, Japan) equipped with the energy dispersive spectrometer (EDS). The UV absorption properties of the bioinks were tested by an ultraviolet-visible near-infrared spectrophotometer

(SolidSpec-3700, Shimadzu, Japan), and the wavelength range of the test was 275–450 nm. The dynamic viscosity of bioink at variable shear rate of 0–1000 s⁻¹ was measured by rheometer (Mars60, Haake, Germany). Phase components of the powders were analyzed using an X-ray diffractometer (XRD-7000, Shimadzu Company, Japan) with a detection range of 5–80° and a scan speed of 5° per minute. The chemical bonds of the samples were detected by a fourier transform infrared spectroscopy (Nicolet, iS50R, Thermo, Scientific, USA), collecting at wavenumbers ranging from 4000 to 500 cm⁻¹.

2.5. Mechanical Test of Scaffolds

The compression tests were performed on an electronic dynamic and static fatigue testing machine (E1000, ITW Instron, USA) at room temperature. The stress (σ) of compression was calculated through Eq. (2.3):

$$\sigma = \frac{F}{A_0} \quad (2.3)$$

where F and A_0 represents the load force and the sample's starting cross-section area perpendicular to the direction of the load force, respectively. Compression modulus (E_c) refers to the ratio of stress and strain of material under compressive force, which is calculated by Eq. (2.4):

$$E_c = \frac{\sigma}{\varepsilon} \quad (2.4)$$

where ε is compressive strain. Generally, E_c equals the slope of the stress-strain curve at the elastic deformation stage, which can be obtained from Origin software. And the energy absorption (E_a) refers to the area enclosed by the stress-strain curve, which is calculated by Eq. (2.5):

$$E_a = \int f(x) dx \quad (2.5)$$

where $f(x)$ is the compressive stress-strain curve. When performing compression tests, the loading speed was set to 2 mm/min. The average of each data point was taken from three tests. To determine the fatigue performance of the support, the cyclic compression test was also set up. The maximum non-destructive strain of each group was determined by previous compression test. For PP, PP/1%BTO, PP/2.5%BTO and PP/5%BTO group, it was set as 50%, 40%, 35%, 30%, respectively. The loading speed was set to 2 mm/s, and the cycle time was ten.

2.6. Electrical Test of Scaffolds

Before the electrical test, the scaffolds need to be polarized under a high electrical field, so that the

electrical effect can be displayed. The scaffolds were polarized by a high-voltage DC power supply (C2s, Dongwen High Voltage, Tianjin, China) with a parameter of -5 kV for 10 min. A cycle-compressed device (E1000, ITW Instron, USA) was used to periodically compress the electrical scaffolds. The voltage output of electrical scaffolds was determined by a digital source table (DMM7510, Keithley, USA). The voltage output of various electrical scaffolds under the same stress was tested first. For testing, attach conductive tape to both sides of the scaffolds and connect to the digital source table. Cyclic compression was applied to the scaffolds, and the compression stress was set to 50 kPa. The loading speed was set to 2 mm/s, and cycle time was 20. Then the effect of different stress on the voltage output was also explored. We tested the voltage output of the PP/5%BTO group at 25, 50, 100 and 200 kPa, with other parameters remaining the same.

2.7. In vitro Swelling Ratio Test

The *in vitro* swelling ratio test was conducted to access the swelling ratio of scaffolds. To remove moisture from scaffolds, freeze-drying was performed. Record the initial mass W_0 using a precision electronic balance (ME403, METTLER TOLEDO, Switzerland). Then, soak scaffolds in a centrifuge tube filled with PBS (pH=7.4) solution. Let stand for 24 hours to fully absorb water to achieve swelling balance. Took it out and dried it with tissue, and then weighed it again to get the mass W_1 after swelling. The swelling rate is calculated by Eq. (2.6):

$$\text{Swelling ratio (\%)} = 100\% \times (W_1 - W_0) / W_0 \quad (2.6)$$

2.8. In vitro Immersion Experiment

The degradability of scaffolds was determined by *in vitro* immersion experiment. The scaffolds were immersed in SBF (pH=7.4) at 37 °C in a shaker for 2, 4, 7 and 14 days, respectively. The ratio of scaffold mass to solution volume was set as 1 g: 10 mL. Finally, the scaffolds were cleaned with deionized water and wiped carefully by tissue. The mass of the degraded scaffolds was measured by a precision electronic balance (ME403, METTLER TOLEDO, Switzerland). The degradation rates were calculated using Eq. (2.7):

$$D_r(\%) = 100\% \times (W_0 - W_i) / W_0 \quad (2.7)$$

where D_r is the degradation rate of the scaffold, and W_0 is the mass of scaffold before immersion. W_i is the mass of scaffold after matching days of SBF immersion.

3. RESULTS AND DISCUSSIONS

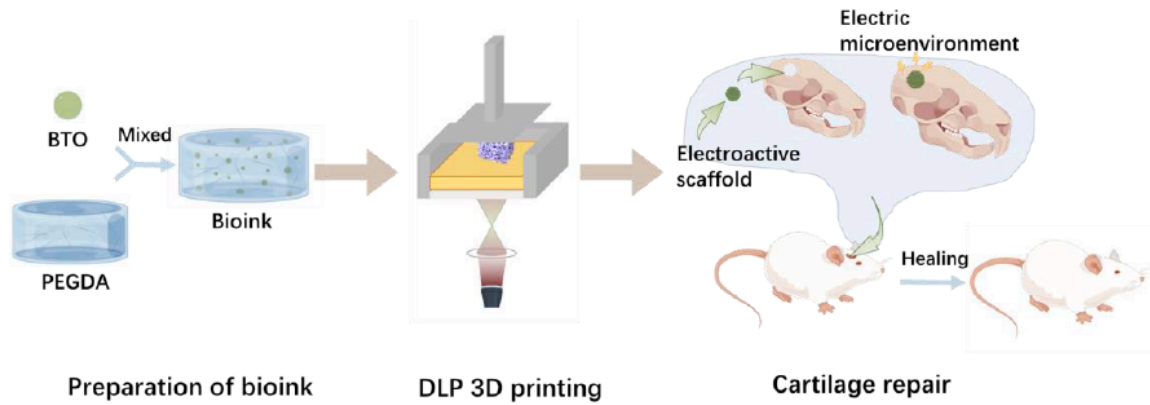


Figure 1: Schematic illustration of the manufacturing of composite scaffold and cartilage repair.

3.1. Characterization of Raw Materials

BTO powders showed a regular shape with an average particle size of about 1 μm (Figure 2A–B). According to the XRD pattern (Figure 2C), the electrical effect is demonstrated by the splitting peak at about 2θ of 45° [40]. The fourier infrared absorption spectra (FT-IR) (Figure 2D) displayed the standard absorption peak of C=O stretching vibration of PEGDA ($\sim 1726\text{ cm}^{-1}$) before and after UV crosslinking [41]. Peaks at 1095 cm^{-1} and 2867 cm^{-1} were ascribed to the chemical structure of PEGDA, -COOR and $-\text{CH}_2$, respectively. Before crosslinking, peaks at 1625 cm^{-1} and 810 cm^{-1} were observed which are characteristic of C=C double bonds but absent after crosslinking.

These results showed that PEGDA was completely polymerized after UV irradiation.

3.2. Fabrication of Scaffolds

Viscosity is an element that plays a crucial role in the DLP 3D printing process [23]. Therefore, it is necessary to explore the viscosity of bioinks first. The viscosity of each group of bioinks was depicted in Figure 3A. At a shear rate of 100 s^{-1} , the viscosity of PP was the lowest at $617.7\text{ mPa}\cdot\text{s}$, while the viscosity of PP/1%BTO was the highest at $730.3\text{ mPa}\cdot\text{s}$. The viscosity of PP/2.5%BTO and PP/5%BTO were $646.4\text{ mPa}\cdot\text{s}$ and $694.4\text{ mPa}\cdot\text{s}$, respectively. After adding

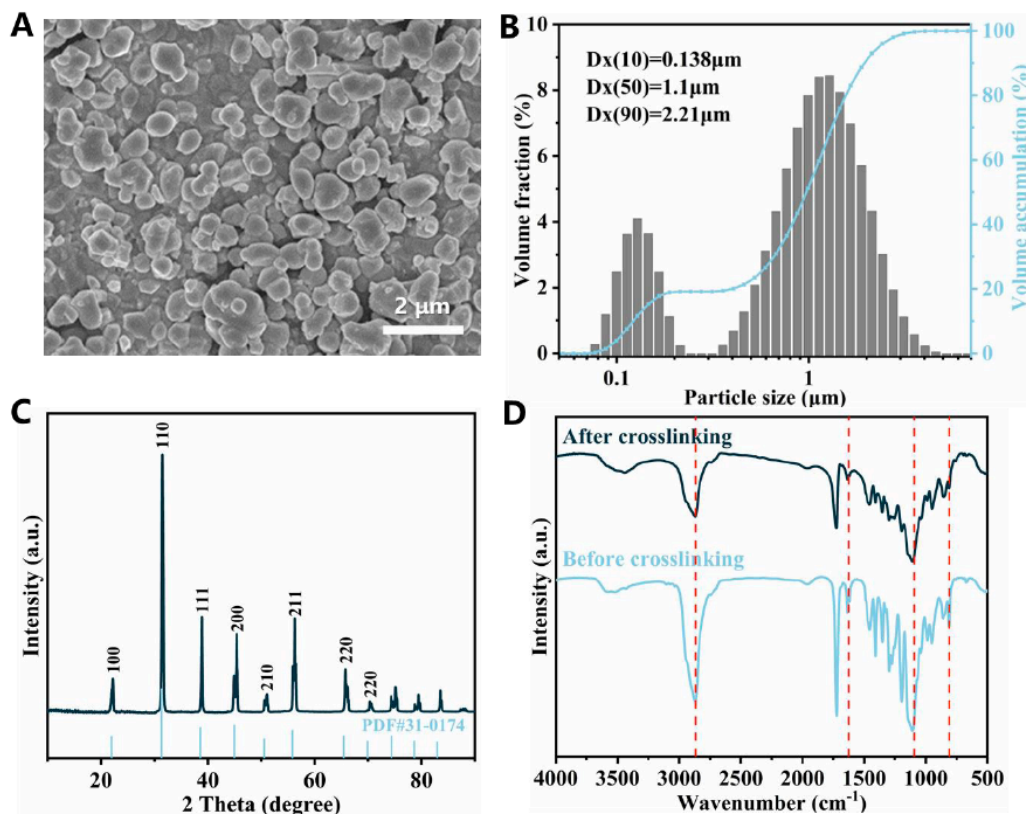


Figure 2: Characterization of raw materials (A) SEM images of BTO powders. (B) particle size distributions of BTO powders. (C) X-ray diffraction spectrum of BTO powders. (D) FT-IR spectra of PEGDA before and after UV crosslinking.

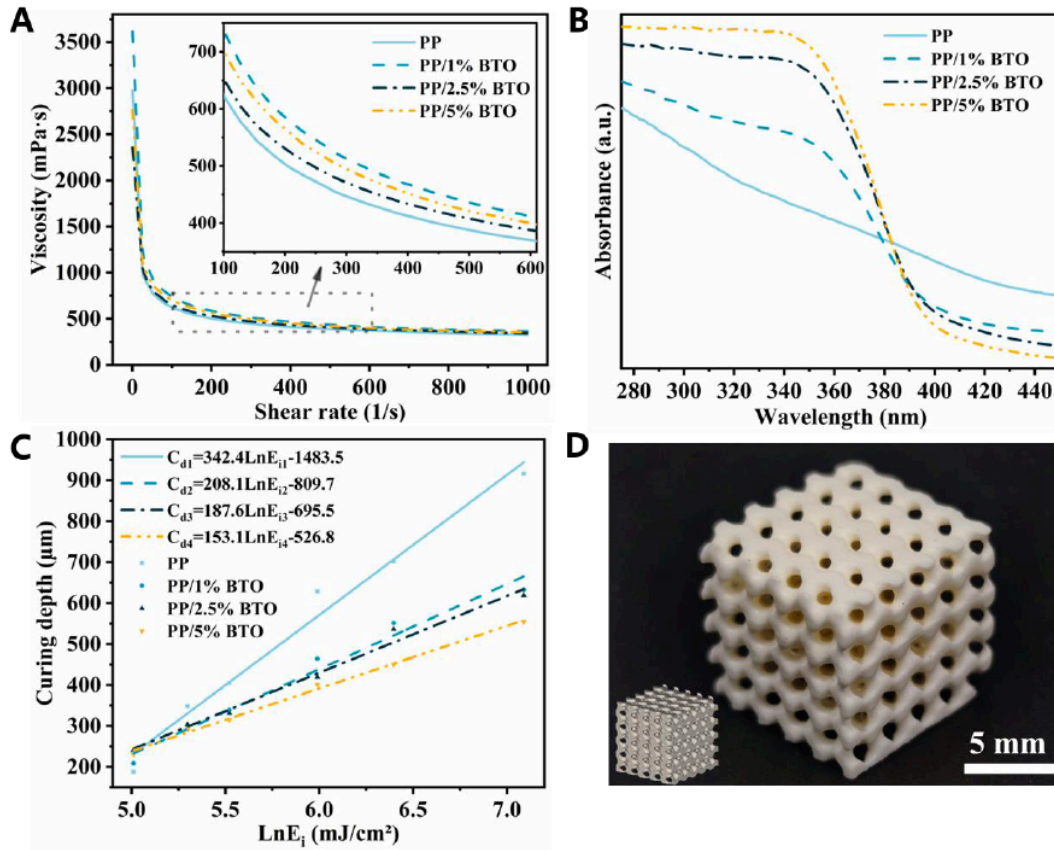


Figure 3: Dynamic viscosity (A) and UV absorption properties (B) of bioinks with different BTO powder content. (C) Curing depth of bioinks at different exposure energies. (D) Photography of one scaffold and its corresponding 3D model picture.

BTO powders, the viscosity of the bioinks was slightly improved, among which PP/1%BTO had the highest viscosity. But in general, the viscosity of bioinks was in the suitable range for DLP 3D printing.

We investigated the UV light absorption of bioinks. As shown in Figure 3B, all bioinks had high UV light absorption values below the wavelength of 350 nm, while the values above 390 nm were already low. Therefore, UV light with a wavelength of 405 nm was chosen as the light source of the DLP 3D printer.

Curing depth and forming precision are the key factors that influence the quality of scaffolds, which are determined by the exposure energy [42]. The relationship between curing depth and exposure energy was tested, and mathematical fitting was done according to Eq. (2.2). The results were shown in Figure 3C. With increasing BTO content, the slope of the fitting Eq. (D_p) gradually decreased, which meant it required more exposure energy to obtain a certain curing depth. While the excess exposure energy would cause poor forming accuracy. Taking both into consideration, the exposure energy of PP, PP/1%BTO, PP/2.5%BTO and PP/5%BTO was selected as 240, 300, 320 and 360 mJ/cm², respectively.

The successful printing PP/5%BTO scaffold is shown in Figure 3D. The small picture in the lower left

corner of Figure 3D is the 3D model corresponding to the scaffold. The scaffold accurately restored the model, and some details, such as the aperture, are preserved, indicating that the printing parameters are suitable.

3.3. Characterization of Scaffolds

The microstructure of composite scaffolds is shown in Figure 4A. The surface of PP scaffolds was very smooth, while the surface of other scaffolds with BTO added showed the presence of BTO particles. The surface roughness of the scaffolds increased as the amount of BTO particles increased. Simultaneously, there were several small holes scattered across the surface of the scaffold, showing that the composite scaffolds had a porous structure that was advantageous for cell adhesion and growth [43, 44]. According to Figure 4B–C, EDS mapping of the PP/5%BTO showed that the special elements (Ba and Ti present in BTO) were uniformly distributed, indicating that BTO particles were evenly distributed in the scaffolds.

The scaffolds' FT-IR spectra are shown in Figure 4D. The peak at 810 cm⁻¹ which represented the C=C double bond vanished indicating PEGDA was completely polymerization. As the BTO content grew,

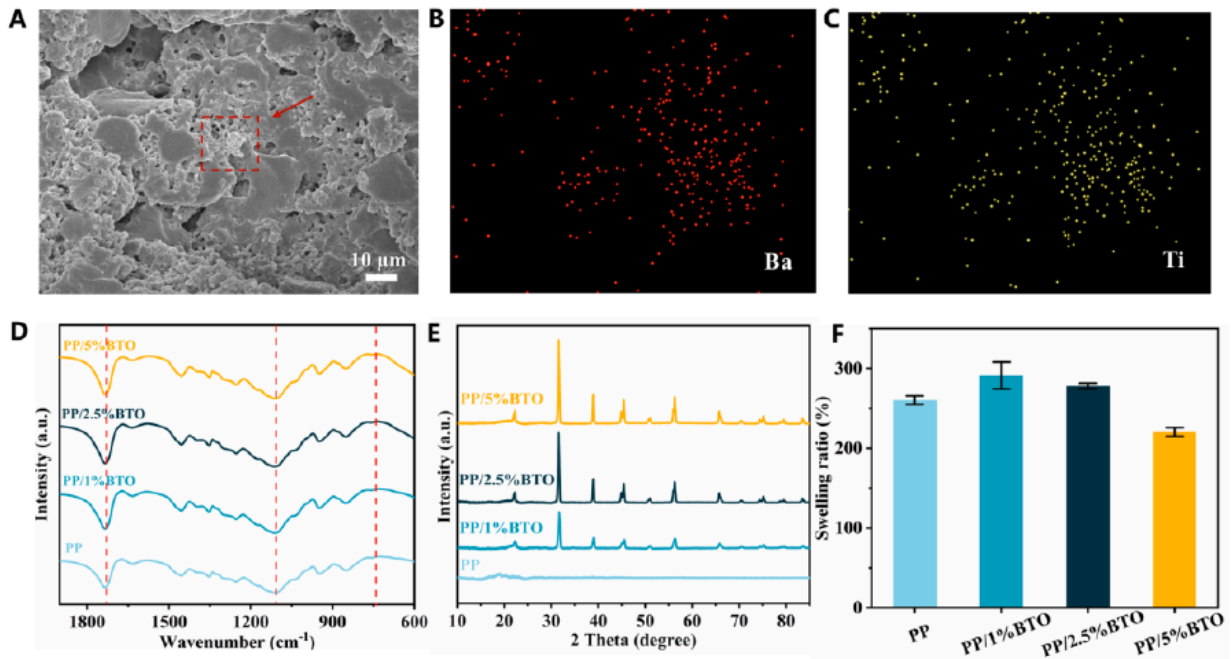


Figure 4: (A) SEM of PP/5%BTO. (B) Element distribution of scaffold (Ba). (C) Element distribution of scaffold (Ti). FT-IR spectra (D), X-ray diffraction spectrum (E) and swelling ratio (F) of each group of scaffolds.

so did the strength of the peak at 1100 cm^{-1} . The whole curve exhibited a minor move to the right, indicating that there were few hydrogen bonds formed.

The X-ray diffraction spectra of scaffolds are shown in Figure 4E. In addition to PP, the characteristic peaks of other groups appeared at 21.98° , 31.36° , 38.64° and so on, which positions were as same as those of BTO powders showed in Figure 2C. The splitting peak at about 2θ of 45° can also be observed in PP/1%BTO, PP/2.5%BTO and PP/5%BTO, which demonstrated the electrical properties of scaffolds. Furthermore, the strength of the characteristic peaks rose as BTO content in the scaffolds increased, and this meant the improvement of the electrical properties of scaffolds with the increase of BTO powder content.

The ideal scaffolds should be able to absorb fluid buildup from cartilage damage and maintain moist microenvironment [45]. The swelling rate of the scaffolds is shown in Figure 4D. After soaking in PBS for 24 hours to achieve swelling equilibrium, there was little difference in the swelling rate among the four groups. The swelling rate of the PP/1%BTO was the highest, which was 291%. With the increase of BTO content, the expansion rate gradually decreased, and swelling rate of the PP/5%BTO was already lower than that of the PP. In general, the swelling rate of the scaffolds was to meet the clinical requirements.

3.4. Mechanical Properties of Scaffolds

The ideal electrical cartilage scaffolds should have similar mechanical properties to human cartilage[46],

which has certain strength, elasticity, and fatigue properties [47]. The mechanical properties of the scaffolds were indicated by the compression test. The scaffolds' compressive stress-strain curves are depicted in Figure 5A. A photograph of the compression test is also contained. Compared with PP, the strength of other groups had improved. As the content of BTO increased, the compressive strength of scaffolds improved. The strength of PP/5%BTO was increased by three times. The compression modulus also had the same trend as shown in Figure 5B. Compared with PP, modulus of other groups had improved, too. Among them, the modulus of PP/5%BTO almost doubled. The energy absorption of scaffolds is shown in Figure 5C. The addition of BTO powders increased the energy absorption of scaffolds several times, and PP/5%BTO had the highest increase, which was almost five times higher than PP. The addition of BTO powders made composite scaffolds possess a superior ability to resist deformation.

Cyclic compression tests were carried out to determine the fatigue properties of the scaffolds. The result of PP/1%BTO is shown in Figure 5D and results of other groups can be found in supplementary information. Results showed that the PP/1%BTO could tolerated consecutive loading-unloading deformation for ten cycles at 40% strain, demonstrating that the scaffolds had sufficient damage tolerance under pressure. However, to complete ten cycles, the strain of PP/2.5%BTO and PP/5%BTO must not exceed 35% and 30%, respectively. Of course, the bigger the scaffold's BTO powder content, the greater the force

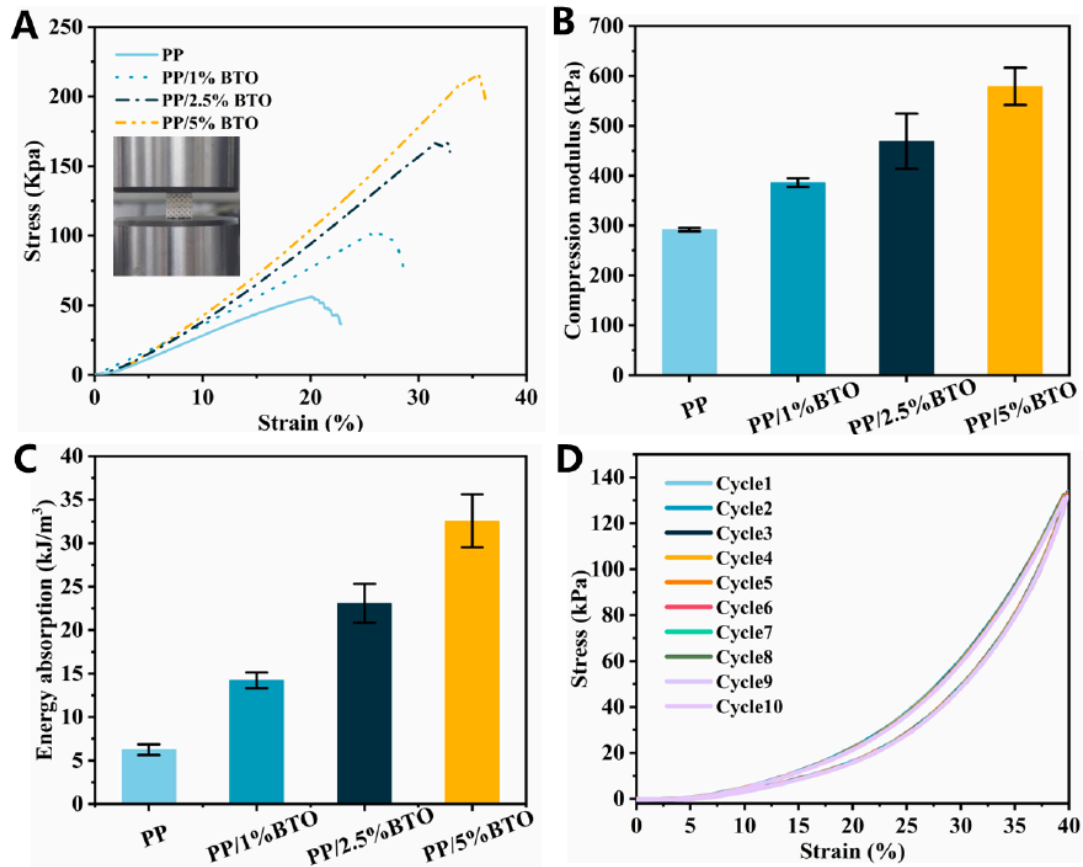


Figure 5: Mechanical properties of scaffolds. (A) Compressive stress-strain curves. (B) Compression modulus. (C) Energy absorption. (D) Cyclic compression curve of PP/1%BTO.

required to generate the same strain. All results revealed that the addition of BTO powders significantly improved the mechanical strength of the scaffolds while having some negative effects on the fatigue characteristics. Therefore, it's significant to determine the amount of BTO powders added so that the scaffolds can achieve an excellent balance between mechanical properties and flexibility.

3.5. Electrical Properties of Scaffolds

To detect the electrical properties of scaffolds, a voltage output test was performed. As shown in Figure 6A, PP as a control also exhibited a tiny voltage of 3 mV under pressure. This may be due to the triboelectricity generated by the scaffolds and conductive tape during compression. Figure 6A shows that after BTO powders were added, all scaffolds had a certain voltage output, which was a manifestation of an electrical effect. The voltage output of the PP/1%BTO, PP/2.5%BTO and PP/5%BTO were approximately 50, 75 and 100 mV, respectively. It can be known that with the increase of BTO content, the voltage output of the scaffolds increased. Therefore, to improve the voltage output of the scaffolds, increasing the amount of BTO powders added is an effective way. However, according to results in Section 3.3, the addition of

excessive BTO powders will have some negative effects on the mechanical properties. According to the situation to determining the proportion of added BTO powders so that the voltage output and mechanical properties are in line with the cartilage scaffold requirements is the most reasonable.

Further, the influence of different stress on the voltage output of scaffolds was also investigated. PP/5%BTO was selected as the representative of this part for the test. As shown in Figure 6B, they demonstrated the voltage output of scaffolds at stress of 25, 50, 100 and 200 kPa, respectively. There is a clear relationship between the voltage output and the applied stress. When the stress increased, the voltage output also improved. Initially we got a voltage output of 100 mV under stress of 50 kPa. When the stress increased to 100 kPa, the voltage output correspondingly increased to 150 mV. Then, when the stress further increased to 200 kPa, the voltage output also reached 300 mV, which was three times the initial value. Similarly, when the stress was reduced to 25 kPa, the voltage output was also reduced to only 50 mV. This showed that in addition to changing the proportion of added powders, the voltage output of scaffolds can be controlled by adjusting the applied stress.

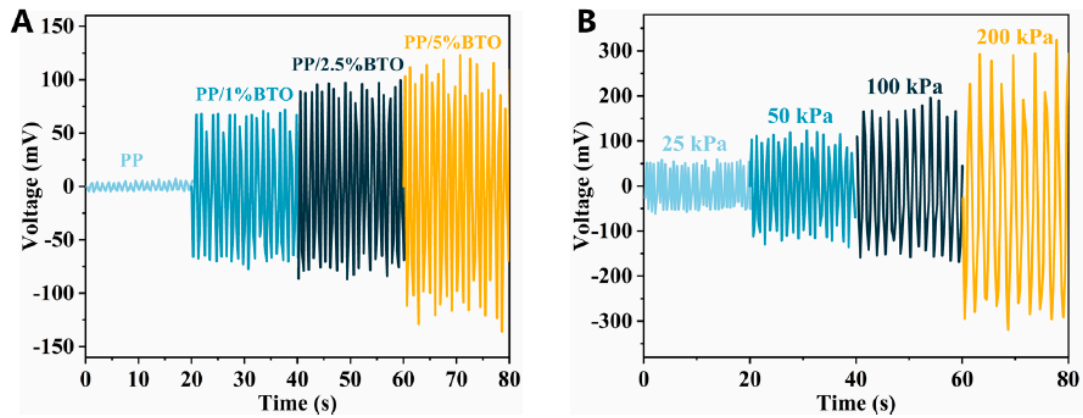


Figure 6: Electrical properties of scaffolds. (A) Voltage output of scaffolds under 50kPa stress. (B) Voltage output of PP/5%BTO under different stress.

3.6. *In Vitro* Degradation

Biomaterials must have good biodegradability to be broken down and absorbed in the human body [48, 49]. The degradation ratio of all groups is shown in Figure 7. All scaffolds are degradable. After 14 days of SBF immersion, the degradation rate of PP was 2.8%. The degradation rate of other groups with BTO powders was higher than that of PP. The highest degradation rate was 7.1% in PP/2.5%BTO. This could be because the inclusion of BTO powders increased the number of holes within the scaffolds. The degradation speed of scaffolds in different stages was also different. In the first four days, the degradation rate of the scaffold was faster. After that, the degradation rate slowed down. In general, the degradation rate of scaffolds was relatively slow. These results indicated that the composite scaffolds have good degradability and may be an ideal choice for cartilage repair.

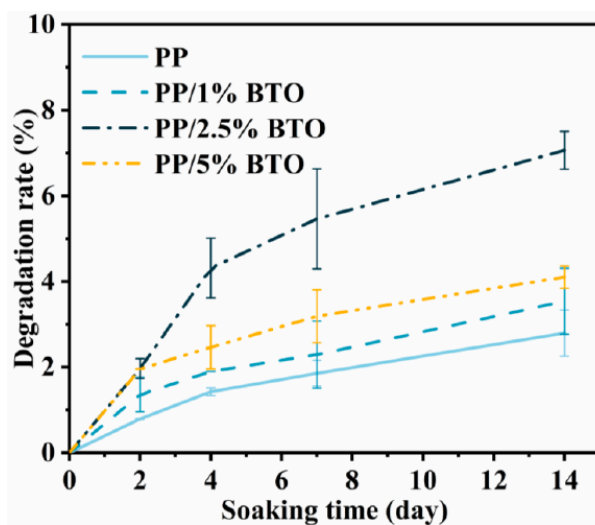


Figure 7: Degradation rate of scaffolds.

4. CONCLUSION

In this study, we created photocurable hydrogel/BaTiO₃ composite bioinks with viscosity and

other parameters suitable for DLP 3D printing. Then a DLP 3D printer was utilized to fabricate composite cartilage scaffolds with highly improved mechanical, electrical, and degradable properties. The inclusion of BaTiO₃ powders was discovered to significantly improve the mechanical characteristics of hydrogel scaffolds. Compared with pure hydrogel, the mechanical strength of composite scaffolds rose threefold, the compression modulus doubled, and the energy absorption increased fivefold. Mechanical property enhancements could increase the stability of cartilage scaffolds and wide their application situations. Besides, the composite scaffolds exhibited superior electrical properties, with a voltage output of 100 mV which was two orders of magnitude greater than that of pure hydrogels. As a result, the composite scaffolds can generate an electrical microenvironment comparable to that seen inside the human body which plays a critical function in stimulating cartilage regeneration and remodeling. Furthermore, the composite scaffolds also had a high degradation rate which reached 7% after 14 days of SBF immersion. This lays the groundwork for the *in vivo* implantation of composite cartilage scaffolds. In general, the hydrogel/BaTiO₃ composite scaffolds have improved mechanical properties, excellent electrical properties, and superior properties. We believe it will contribute to the clinical treatment of cartilage injury.

ACKNOWLEDGMENTS

The authors would like to thank the State Key Laboratory of Materials Processing and Die & Mould Technology for their assistance in SEM, XRD, and mechanical tests. The author would also like to thank the Analytical and Testing Center of Huazhong University of Science and Technology for their assistance in ultraviolet light absorption and fourier transforms infrared spectrometer characterization.

FUNDING

This work was supported by grants from the National Natural Science Foundation of China (52205363), Fundamental Research Funds for the Central Universities (2019kfyRCPY044 and 2021GCRC002), Program for HUST Academic Frontier Youth Team (2018QYTD04), Program for Innovative Research Team of the Ministry of Education (IRT1244).

DECLARATION OF COMPETING INTEREST

The authors declare that they have no known competing financial interests or personal relationships that could have appeared to influence the work reported in this paper.

DATA AVAILABILITY

Data will be made available on reasonable request.

REFERENCES

- [1] "Prevalence of Doctor-Diagnosed Arthritis and Arthritis-Attributable Activity Limitation—United States, 2003-2005," *JAMA*, vol. 296, no. 22, p. 2671, Dec. 2006. <https://doi.org/10.1001/jama.296.22.2671>
- [2] I. A. Vaughn, E. L. Terry, E. J. Bartley, N. Schaefer, and R. B. Fillingim, "Racial-Ethnic Differences in Osteoarthritis Pain and Disability: A Meta-Analysis," *J. Pain*, vol. 20, no. 6, pp. 629-644, Jun. 2019. <https://doi.org/10.1016/j.jpain.2018.11.012>
- [3] M. Liu *et al.*, "Injectable hydrogels for cartilage and bone tissue engineering," *Bone Res.*, vol. 5, no. 1, p. 17014, May 2017. <https://doi.org/10.1038/boneres.2017.14>
- [4] Z. Zhou, J. Zheng, X. Meng, and F. Wang, "Effects of Electrical Stimulation on Articular Cartilage Regeneration with a Focus on Piezoelectric Biomaterials for Articular Cartilage Tissue Repair and Engineering," *Int. J. Mol. Sci.*, vol. 24, no. 3, p. 1836, Jan. 2023. <https://doi.org/10.3390/ijms24031836>
- [5] H. Li *et al.*, "The Application of Hyaluronic Acid-Based Hydrogels in Bone and Cartilage Tissue Engineering," *Adv. Mater. Sci. Eng.*, vol. 2019, pp. 1-12, Dec. 2019. <https://doi.org/10.1155/2019/3027303>
- [6] S. Van Vlierberghe, P. Dubruel, and E. Schacht, "Biopolymer-Based Hydrogels As Scaffolds for Tissue Engineering Applications: A Review," *Biomacromolecules*, vol. 12, no. 5, pp. 1387-1408, May 2011. <https://doi.org/10.1021/bm200083n>
- [7] B. Choi, S. Kim, B. Lin, B. M. Wu, and M. Lee, "Cartilaginous Extracellular Matrix-Modified Chitosan Hydrogels for Cartilage Tissue Engineering," *ACS Appl. Mater. Interfaces*, vol. 6, no. 22, pp. 20110-20121, Nov. 2014. <https://doi.org/10.1021/am505723k>
- [8] M. Yazdimaghani *et al.*, "Hybrid Macroporous Gelatin/Bioactive-Glass/Nanosilver Scaffolds with Controlled Degradation Behavior and Antimicrobial Activity for Bone Tissue Engineering," *J. Biomed. Nanotechnol.*, vol. 10, no. 6, pp. 911-931, Jun. 2014. <https://doi.org/10.1166/jbn.2014.1783>
- [9] B. V. Slaughter, S. S. Khurshid, O. Z. Fisher, A. Khademhosseini, and N. A. Peppas, "Hydrogels in Regenerative Medicine," *Adv. Mater.*, vol. 21, no. 32-33, pp. 3307-3329, Sep. 2009. <https://doi.org/10.1002/adma.200802106>
- [10] M. Liu *et al.*, "Injectable hydrogels for cartilage and bone tissue engineering," *Bone Res.*, vol. 5, no. 1, p. 17014, May 2017. <https://doi.org/10.1038/boneres.2017.14>
- [11] Y. Wei *et al.*, "A novel injectable scaffold for cartilage tissue engineering using adipose-derived adult stem cells," *J. Orthop. Res.*, vol. 26, no. 1, pp. 27-33, Jan. 2008. <https://doi.org/10.1002/jor.20468>
- [12] A. Sivashanmugam, R. Arun Kumar, M. Vishnu Priya, S. V. Nair, and R. Jayakumar, "An overview of injectable polymeric hydrogels for tissue engineering," *Eur. Polym. J.*, vol. 72, pp. 543-565, Nov. 2015. <https://doi.org/10.1016/j.eurpolymj.2015.05.014>
- [13] H. Tan, H. Li, J. P. Rubin, and K. G. Marra, "Controlled gelation and degradation rates of injectable hyaluronic acid-based hydrogels through a double crosslinking strategy," *J. Tissue Eng. Regen. Med.*, vol. 5, no. 10, pp. 790-797, Nov. 2011. <https://doi.org/10.1002/term.378>
- [14] R. Jin *et al.*, "Injectable chitosan-based hydrogels for cartilage tissue engineering," *Biomaterials*, vol. 30, no. 13, pp. 2544-2551, May 2009. <https://doi.org/10.1016/j.biomaterials.2009.01.020>
- [15] G. Liu *et al.*, "Fabrication and characterization of SiC/Al composites prepared by laser powder bed fusion (LPBF) combined with vacuum pressure infiltration," *Mater. Des.*, vol. 236, p. 112495, Dec. 2023. <https://doi.org/10.1016/j.matdes.2023.112495>
- [16] A.-N. Chen *et al.*, "High-performance ceramic parts with complex shape prepared by selective laser sintering: a review," *Adv. Appl. Ceram.*, vol. 117, no. 2, pp. 100-117, Feb. 2018. <https://doi.org/10.1080/17436753.2017.1379586>
- [17] A.-N. Chen *et al.*, "High-porosity mullite ceramic foams prepared by selective laser sintering using fly ash hollow spheres as raw materials," *J. Eur. Ceram. Soc.*, vol. 38, no. 13, pp. 4553-4559, Oct. 2018. <https://doi.org/10.1016/j.jeurceramsoc.2018.05.031>
- [18] C. Wang *et al.*, "3D printed porous biomass-derived SiCnw/SiC composite for structure-function integrated electromagnetic absorption," *Virtual Phys. Prototyp.*, vol. 17, no. 3, pp. 718-733, Jul. 2022. <https://doi.org/10.1080/17452759.2022.2056950>
- [19] A.-N. Chen *et al.*, "TEM analysis and mechanical strengthening mechanism of MnO₂ sintering aid in selective laser sintered porous mullites," *J. Alloys Compd.*, vol. 809, p. 151809, Nov. 2019. <https://doi.org/10.1016/j.jallcom.2019.151809>
- [20] J. Li, C. Wu, P. K. Chu, and M. Gelinsky, "3D printing of hydrogels: Rational design strategies and emerging biomedical applications," *Mater. Sci. Eng. R Rep.*, vol. 140, p. 100543, Apr. 2020. <https://doi.org/10.1016/j.mser.2020.100543>
- [21] K. Markstedt, A. Mantas, I. Tournier, H. Martínez Ávila, D. Hägg, and P. Gatenholm, "3D Bioprinting Human Chondrocytes with Nanocellulose-Alginate Bioink for Cartilage Tissue Engineering Applications," *Biomacromolecules*, vol. 16, no. 5, pp. 1489-1496, May 2015. <https://doi.org/10.1021/acs.biomac.5b00188>
- [22] W. Shi *et al.*, "Structurally and Functionally Optimized Silk-Fibroin-Gelatin Scaffold Using 3D Printing to Repair Cartilage Injury In vitro and In vivo," *Adv. Mater.*, vol. 29, no. 29, p. 1701089, Aug. 2017. <https://doi.org/10.1002/adma.201701089>
- [23] J. Huh, Y.-W. Moon, J. Park, A. Atala, J. J. Yoo, and S. J. Lee, "Combinations of photoinitiator and UV absorber for cell-based digital light processing (DLP) bioprinting," *Biofabrication*, vol. 13, no. 3, p. 034103, Jul. 2021. <https://doi.org/10.1088/1758-5090/abfd7a>
- [24] H. Quan, T. Zhang, H. Xu, S. Luo, J. Nie, and X. Zhu, "Photo-curing 3D printing technique and its challenges," *Bioact. Mater.*, vol. 5, no. 1, pp. 110-115, Mar. 2020. <https://doi.org/10.1016/j.bioactmat.2019.12.003>
- [25] K. Yue, G. Trujillo-de Santiago, M. M. Alvarez, A. Tamayo, N. Annabi, and A. Khademhosseini, "Synthesis, properties, and

- biomedical applications of gelatin methacryloyl (GelMA) hydrogels," *Biomaterials*, vol. 73, pp. 254-271, Dec. 2015. <https://doi.org/10.1016/j.biomaterials.2015.08.045>
- [26] P. Chen *et al.*, "Desktop-stereolithography 3D printing of a radially oriented extracellular matrix/mesenchymal stem cell exosome bioink for osteochondral defect regeneration," *Theranostics*, vol. 9, no. 9, pp. 2439-2459, 2019. <https://doi.org/10.7150/thno.31017>
- [27] P. Feng *et al.*, "Structural and Functional Adaptive Artificial Bone: Materials, Fabrications, and Properties," *Adv. Funct. Mater.*, vol. 33, no. 23, p. 2214726, Jun. 2023. <https://doi.org/10.1002/adfm.202214726>
- [28] C. Yan *et al.*, "Additive manufacturing of hydroxyapatite and its composite materials: A review," *J. Micromechanics Mol. Phys.*, vol. 05, no. 03, p. 2030002, Sep. 2020. <https://doi.org/10.1142/S2424913020300029>
- [29] C. A. L. Bassett, "Biologic significance of piezoelectricity," *Calcif. Tissue Res.*, vol. 1, no. 1, pp. 252-272, Dec. 1967. <https://doi.org/10.1007/BF02008098>
- [30] B. A. C. Housmans *et al.*, "Direct comparison of non-osteoarthritic and osteoarthritic synovial fluid-induced intracellular chondrocyte signaling and phenotype changes," *Osteoarthritis Cartilage*, vol. 31, no. 1, pp. 60-71, Jan. 2023. <https://doi.org/10.1016/j.joca.2022.09.004>
- [31] Schlegel, "Scaffold-dependent differentiation of human articular chondrocytes," *Int. J. Mol. Med.*, Jan. 1998. <https://doi.org/10.3892/ijmm.00000074>
- [32] Y. Li *et al.*, "Strontium-doped calcium silicate scaffolds with enhanced mechanical properties and tunable biodegradability fabricated by vat photopolymerization," *Int. J. Bioprinting*, vol. 9, no. 6, p. 1233, Sep. 2023. <https://doi.org/10.36922/ijb.1233>
- [33] Y. Liu *et al.*, "Exercise-induced piezoelectric stimulation for cartilage regeneration in rabbits," *Sci. Transl. Med.*, vol. 14, no. 627, p. eabi7282, Jan. 2022. <https://doi.org/10.1126/scitranslmed.abi7282>
- [34] A. Chen *et al.*, "Multi-Material 3D and 4D Bioprinting of Heterogeneous Constructs for Tissue Engineering," *Adv. Mater.*, p. 2307686, Sep. 2023.
- [35] J. Su *et al.*, "Three-dimensional printing of gyroid-structured composite bioceramic scaffolds with tuneable degradability," *Biomater. Adv.*, vol. 133, p. 112595, Feb. 2022. <https://doi.org/10.1016/j.msec.2021.112595>
- [36] J. Jacob, N. More, K. Kalia, and G. Kapusetti, "Piezoelectric smart biomaterials for bone and cartilage tissue engineering," *Inflamm. Regen.*, vol. 38, no. 1, p. 2, Dec. 2018. <https://doi.org/10.1186/s41232-018-0059-8>
- [37] A. Chen *et al.*, "3D/4D printed bio-piezoelectric smart scaffolds for next-generation bone tissue engineering," *Int. J. Extreme Manuf.*, vol. 5, no. 3, p. 032007, Sep. 2023. <https://doi.org/10.1088/2631-7990/acd88f>
- [38] C. Yan, L. Hao, A. Hussein, and P. Young, "Ti-6Al-4V triply periodic minimal surface structures for bone implants fabricated via selective laser melting," *J. Mech. Behav. Biomed. Mater.*, vol. 51, pp. 61-73, Nov. 2015. <https://doi.org/10.1016/j.jmbbm.2015.06.024>
- [39] S. Zakeri, M. Vippola, and E. Levänen, "A comprehensive review of the photopolymerization of ceramic resins used in stereolithography," *Addit. Manuf.*, vol. 35, p. 101177, Oct. 2020. <https://doi.org/10.1016/j.addma.2020.101177>
- [40] D. Liu *et al.*, "Ultrasound-triggered piezocatalytic composite hydrogels for promoting bacterial-infected wound healing," *Bioact. Mater.*, vol. 24, pp. 96-111, Jun. 2023. <https://doi.org/10.1016/j.bioactmat.2022.11.023>
- [41] M. Kumar, S. Ghosh, V. Kumar, V. Sharma, and P. Roy, "Tribo-mechanical and biological characterization of PEGDA/bioceramics composites fabricated using stereolithography," *J. Manuf. Process.*, vol. 77, pp. 301-312, May 2022. <https://doi.org/10.1016/j.jmapro.2022.03.024>
- [42] G. Qi, Y. Zeng, and J. Chen, "Preparation of porous SnO₂-based ceramics with lattice structure by DLP," *Ceram. Int.*, vol. 48, no. 10, pp. 14568-14577, May 2022. <https://doi.org/10.1016/j.ceramint.2022.01.350>
- [43] Y. Zhou *et al.*, "Highly Stretchable, Elastic, and Ionic Conductive Hydrogel for Artificial Soft Electronics," *Adv. Funct. Mater.*, vol. 29, no. 1, p. 1806220, Jan. 2019. <https://doi.org/10.1002/adfm.201806220>
- [44] K. Nešović *et al.*, "Chitosan-based hydrogel wound dressings with electrochemically incorporated silver nanoparticles - In vitro study," *Eur. Polym. J.*, vol. 121, p. 109257, Dec. 2019. <https://doi.org/10.1016/j.eurpolymj.2019.109257>
- [45] A. I. Raafat, N. M. El-Sawy, N. A. Badawy, E. A. Mousa, and A. M. Mohamed, "Radiation fabrication of Xanthan-based wound dressing hydrogels embedded ZnO nanoparticles: In vitro evaluation," *Int. J. Biol. Macromol.*, vol. 118, pp. 1892-1902, Oct. 2018. <https://doi.org/10.1016/j.ijbiomac.2018.07.031>
- [46] C. Shuai, W. Yang, P. Feng, S. Peng, and H. Pan, "Accelerated degradation of HAP/PLLA bone scaffold by PGA blending facilitates bioactivity and osteoconductivity," *Bioact. Mater.*, vol. 6, no. 2, pp. 490-502, Feb. 2021. <https://doi.org/10.1016/j.bioactmat.2020.09.001>
- [47] B. Tandon, J. J. Blaker, and S. H. Cartmell, "Piezoelectric materials as stimulatory biomedical materials and scaffolds for bone repair," *Acta Biomater.*, vol. 73, pp. 1-20, Jun. 2018. <https://doi.org/10.1016/j.actbio.2018.04.026>
- [48] M. Farokhi, F. Jonidi Shariatzadeh, A. Solouk, and H. Mirzadeh, "Alginate Based Scaffolds for Cartilage Tissue Engineering: A Review," *Int. J. Polym. Mater. Polym. Biomater.*, vol. 69, no. 4, pp. 230-247, Mar. 2020. <https://doi.org/10.1080/00914037.2018.1562924>
- [49] M. N. Collins and C. Birkinshaw, "Hyaluronic acid based scaffolds for tissue engineering-A review," *Carbohydr. Polym.*, vol. 92, no. 2, pp. 1262-1279, Feb. 2013. <https://doi.org/10.1016/j.carbpol.2012.10.028>

Received on 07-11-2023

Accepted on 11-12-2023

Published on 27-12-2023

DOI: <https://doi.org/10.12974/2311-8717.2023.11.07>© 2023 Zhang *et al.*

This is an open access article licensed under the terms of the Creative Commons Attribution Non-Commercial License (<http://creativecommons.org/licenses/by-nc/3.0/>) which permits unrestricted, non-commercial use, distribution and reproduction in any medium, provided the work is properly cited.